JOURNAL OF Materials CHEMISTRY

Synthesis and characterization of composite molecular sieves comprising zeolite Beta with MCM-41 structures

Wanping Guo,[a] Chunrong Xiong,[b] Limin Huang[a] and Quanzhi Li*[a]

[a]*Department of Chemistry, Fudan University, Shanghai 200433, P. R. China. E-mail: qzli@fudan.edu.cn*
[b]*Shanghai Research Institute of Petrochemical Technology, 201208, P. R. China*

Received 12th December 2000, Accepted 12th April 2001
First published as an Advance Article on the web 31st May 2001

Zeolite Beta/MCM-41 composites have been prepared with various crystallinities of zeolite Beta through a two-step crystallization process involving the combination of low crystallinity zeolite Beta synthesis gel with cetyltrimethylammonium bromide surfactant solution. The composites are characterized by XRD, SEM, ^{29}Si and ^{27}Al MAS NMR, N_2 adsorption, NH_3-TPD and catalytic cracking. The experimental results show that the relative crystallinity of Beta in the composites greatly affects the morphology and surface acidity of the materials, while exhibiting similar ^{29}Si, ^{27}Al MAS NMR spectra and N_2 adsorption–desorption isotherms. The pore structural data indicate that the composites contain bimodal mesopore systems and microporous structures of zeolite Beta. Although the number of weak acid sites on the composites with various crystallinities of Beta is comparable, composites with higher Beta crystallinity possess more medium acid sites and show higher catalytic activity for n-heptane cracking.

1. Introduction

The mesoporous molecular sieve MCM-41, one member of the mesoporous M41S materials discovered by researchers at Mobil Corporation,[1,2] has attracted considerable attention because of its uniform mesopores, high surface area and thermal stability. The acid strength of MCM-41 is, however, rather weak compared to traditional zeolites owing to the amorphous character of the MCM-41 framework.[3–5] Microporous molecular sieves such as zeolite Y, ZSM-5 and Beta, have played important roles in acid catalysis because of their peculiar pore structures and strong intrinsic acidities. Unfortunately, under the restriction of small pore sizes, such crystalline microporous materials are not suitable as catalysts for processing large molecules such as those existing in vacuum gas oil which need to be cracked.[6,7] Thus, great interest has been generated in the synthesis of composite materials which combine the performances of both mesoporous and microporous molecular sieves. Up to now, there have been only a few articles involving this issue.[8–11] Kloetstra *et al.*[8] first reported zeolite faujasite coated with a thin layer of mesoporous MCM-41 prepared by a one-step successive synthesis of FAU followed by MCM-41 on FAU, or by adding FAU crystals to a MCM-41 synthesis gel. Later, their attempts to crystallize the walls of mesoporous MCM-41 led to the formation of a material with increased catalytic activity.[9,10] Although FTIR spectra revealed embryonic stages of tectosilicate formation, XRD patterns showed no crystalline features of zeolite.[10] Other studies[11] have been carried out to demonstrate the *in situ* formation of micro- and meso-porous structures of MFI and MCM-41 using a two-template synthesis gel system. Characterization, however, showed that composites of MCM-41/MFI featured fairly complex aggregates of MFI and MCM-41 type material.[11] Recently, ZSM-5/MCM-41 composites were successfully prepared using a dual templating method through a process of a two-step crystallization in our group.[12,13] By this approach, self-assembly using the surfactant cetyltrimethylammonium bromide was first employed to form mesoporous MCM-41. Subsequently, a structure directing agent, tetrapropylammonium bromide, was introduced into the MCM-41 wall through a pretreating process to make the amorphous wall of MCM-41 recrystallize. A solid–solid phase transformation mechanism was put forward to elucidate the recrystallization of the MCM-41 framework.[13] Nevertheless, it is difficult to extend the synthetic method mentioned above to obtain composite materials with zeolite Beta micropores and MCM-41 mesopores because of the solution-mediated transport mechanism for zeolite Beta synthesis.[14] In addition, the high alkalinity ($pH > 12$) of the synthetic mixture for the crystallization of zeolite Beta[15,16] readily leads to the collapse of the mesoporous framework of MCM-41. In order to obtain a Beta/MCM-41 composite, we developed another synthetic approach that was based on the sequential synthesis of colloids of Beta followed by adding the viscous gel to a solution of cetyltrimethylammonium bromide.[17,18] Our studies[18] have revealed that the Beta/MCM-41 composite molecular sieve synthesized in this way possesses a specific mesostructure which is constructed from a large number of secondary building units characteristic of zeolite Beta, originating from the initially crystallized aluminosilicate gel. Moreover, we provide a flexible synthesis of Beta/MCM-41 composite in which the relative amount of the microporous phase of Beta and the Si/Al ratio of the mesoporous phase of MCM-41 can be controlled by varying the crystallization time of the Beta colloid and by supplying the alumina source during the course of the synthesis, respectively.

Herein we describe a series of Beta/MCM-41 composites with various crystallinities of Beta synthesized hydrothermally through a two-step crystallization process *via* combination of low crystallinity zeolite Beta synthesis gel with cetyltrimethylammonium bromide surfactant solution. The structure, acidity and catalytic activity of these Beta/MCM-41 composites is also studied.

2. Experimental

2.1 Preparation of Beta/MCM-41 composites

The sources of silicon and aluminium were fumed silica (Electrochemical Co., Shanghai) and sodium aluminate

 DOI: 10.1039/b009903l

(Jiangpu Chemical Co., Shanghai), respectively. Tetraethylammonium hydroxide solution (TEAOH, 25 wt% aqueous solution, First Chemical Co., Shanghai), cetyltrimethylammonium bromide (CTAB, imported from Denmark) were used as the reagents. In a typical preparation, 0.4 g of sodium aluminate was dissolved in 8.0 g of TEAOH solution, followed by addition of 3.0 g of fumed silica. This mixture was stirred for about 30 min, then transferred into stainless steel autoclaves with hydrothermal treatment at 413 K for 48–192 h. After cooling to room temperature, the colloidal product was added dropwise to 21 g of 14 wt% aqueous CTAB solution with stirring. Subsequently, the pH of the reaction mixture was adjusted to 9.6 by dropwise addition of 50 wt% acetic acid with vigorous stirring. When the addition was over, the slurry was stirred for a further 1 h to obtain a homogeneous gel mixture. This final gel was then loaded into an autoclave and heated at 373 K under autogenous pressure for 48 h. The resulting gel mixture had a chemical composition $1SiO_2$–$0.034Al_2O_3$–$0.05Na_2O$–$0.28TEAOH$–$0.16CTAB$–$27H_2O$. The crystallization was terminated by quenching the autoclave in cold water. The solid product was recovered by filtration and washed with deionized water and dried at 353 K overnight. The organic component was removed by calcining the sample at 823 K for 1 h in flowing nitrogen and then in air for 6 h at the same temperature. Ion exchange of Na-formed Beta/MCM-41 was carried out at 343 K for 2 h with 1 M NH_4NO_3 solution. The protonated form was then obtained by calcining the NH_4^+ form at 773 K for 5 h. By varying the reaction time of the first-step crystallization of Beta at 413 K, four samples were obtained, denoted as S1, S2, S3 and S4 according to the different reaction times of 48 h, 96 h, 144 h and 192 h, respectively.

2.2 Characterization of Beta/MCM-41 composites

The powder X-ray diffraction (XRD) patterns were collected on a Rigaku D/MAX-IIA X-ray powder diffractometer using Ni-filtered Cu Kα radiation at 40 kV and 20 mA. The SiO_2/Al_2O_3 ratio of the samples was determined by chemical analysis using the volume method of potassium fluoride and EDTA titration. Crystallite size and morphology was determined by scanning electron microscopy (HITACHI, S-520). Prior to the SEM measurements, the samples were mounted on a carrier made from glassy carbon and coated with a film of gold.

Solid-state magic angle spinning (MAS) NMR was performed at room temperature on a Bruker MSL-300 spectrometer equipped with a zirconia rotor 7 mm in diameter. The magnetic field was equal to 7.05 T and the spinning frequency was 4.0 kHz. ^{29}Si MAS NMR spectra were recorded at a resonance frequency of 59.63 MHz with a 90° radiofrequency pulse, 7.0 μs excitation pulses, a recycle delay of 1.0 s and a spectral width of 20.0 kHz, whereas ^{27}Al MAS NMR spectra were recorded at a resonance frequency of 78.21 MHz with a 30° radiofrequency pulse, 4.6 μs excitation pulses, a recycle delay of 0.5 s and a spectral width of 29.4 kHz. The chemical shifts were referenced to tetramethylsilane and $AlCl_3 \cdot 6H_2O$ for ^{29}Si and ^{27}Al, respectively.

The N_2 adsorption–desorption isotherms of the samples were measured on a Micromeritics ASAP 2000 apparatus using nitrogen as adsorbate at 77 K. The samples were degassed by gradual heating to 473 K in a vacuum of 0.013 Pa and maintained at this temperature for 3–4 h prior to N_2 adsorption–desorption measurement. The mesoporous structure was analyzed from the desorption branch of the isotherm by the BJH (Barrett–Joyner–Halenda) method using the Halsey equation for multilayer thickness. The micropore area was obtained from the analysis of adsorption branch of the isotherm by the *t*-plot and MP method.[19,20]

NH_3-TPD was carried out in a flow-type fixed-bed reactor with 100 mg of the catalyst employing flowing helium (40 cm^3 min^{-1}) as the carrier gas and a thermoconductor as the detector. The samples inside the TPD reactor were first activated at 773 K for 1 h, followed by adsorption of ammonia at 393 K, then TPD of ammonia was performed at a heating rate of 19 K min^{-1}. The amount of ammonia desorbed from the catalyst was collected in a liquid N_2 trap and quantitatively analyzed by the thermoconductor.

Catalytic activities for n-heptane cracking were tested in a pulse microreactor with a catalyst load of 15 mg (60–80 mesh) after being activated at 673 K for 2 h. Hydrogen was used as the carrier gas at a flow rate of 45 cm^3 min^{-1}. Following this procedure 1 μl of the reactant was injected into the catalyst bed through a microsyringe. The cracking products were analyzed by an on-line gas chromatograph equipped with a flame ionization detector.

3. Results and discussion

The XRD patterns of calcined Beta/MCM-41 composites are shown in Fig. 1. The very typical long-range ordered hexagonal MCM-41 mesoporous phase[2] can be verified by the observation of three distinct diffraction peaks indexed as (100), (110) and (200) in the low 2θ region of 1.5–10°. While in the high 2θ region of 5–35°, diffraction peaks at around 7.6° and 22.4° can be observed, indicating the presence of the Beta phase.[21] Table 1 displays the *d* spacings and relative crystallinity of Beta in the Beta/MCM-41 composites. It can be seen that there is a remarkable shrinkage in the interplanar spacings, d_{100}, of the mesoporous phases in the composites after removal of the organic component by calcination. Moreover, the lower the relative crystallinity of Beta, the more the *d* spacings of the mesoporous phase vary. For instance, after calcination, the interplanar spacing d_{100} of the mesoporous phase in the composite with 39% crystallinity of Beta (S4) shows a shrinkage of 0.28 nm, from 4.53 nm to 4.25 nm, whereas the interplanar spacing d_{100} of the mesoporous phase in the composite with 16% crystallinity of Beta (S1) shrinks from 4.37 nm to 3.91 nm, a decrease of 0.46 nm. However, the *d* spacings of microporous phases in the composites show little variation after calcination.

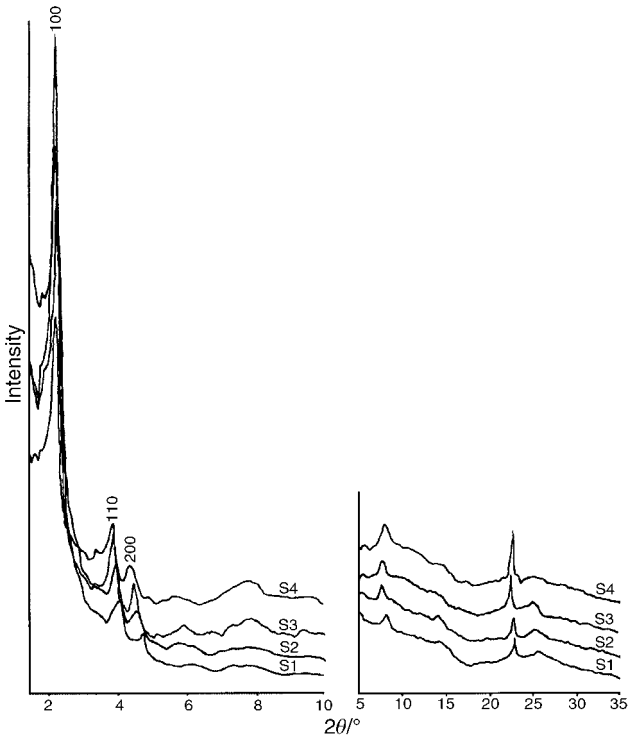

Fig. 1 Powder XRD patterns of calcined Beta/MCM-41 composites for diffraction areas of mesoporous (left) and microporous (right) structures.

Table 1 Summary of *d* spacings and the relative crystallinity of Beta in Beta/MCM-41 composites

	d Spacing/nm										
	Mesoporous phase						Microporous phase				
	As-synthesized			Calcined			As-synthesized		Calcined		
Sample	100	110	200	100	110	200	101	302	101	302	Relative crystallinity[a] (%)
S1	4.37	2.50	2.17	3.91	2.25	1.99	1.18	0.399	1.15	0.396	16
S2	4.48	2.55	2.23	4.07	2.32	2.01	1.18	0.399	1.14	0.396	19
S3	4.44	2.55	2.24	4.23	2.42	2.13	1.17	0.398	1.13	0.397	28
S4	4.53	2.65	2.29	4.25	2.41	2.10	1.17	0.398	1.15	0.397	39

[a]Relative crystallinity is equal to the weight amount of Beta microporous phase in the Beta/MCM-41 composite, which can be deduced from the area of the most intense diffraction peak at 22.4° 2θ in the XRD pattern.[18]

These phenomena show that the decrease of the relative crystallinity of the Beta phase leads to increased shrinkage of the mesophase in Beta/MCM-41 composites.

Scanning electron micrographs of Beta/MCM-41 composites are presented in Fig. 2. It is found that the composite with 16% crystallinity of Beta (sample S1) exhibits loose aggregates embedded within minuscule particles. With the increase of crystallinity of Beta, the discrete particles grow into ball-like grains which can be observed in samples S2 and S3. The micrograph of sample S4 (39% crystallinity of Beta) shows well distributed globular particles with a loose surface. These observations may suggest that the loose aggregates can be assigned to the mesoporous phase and the minuscule particles correspond to the microporous Beta phase which grows into ball-like grains with increasing crystallization time.

^{29}Si MAS NMR and ^{27}Al MAS NMR spectra of Beta/MCM-41 composites are given in Figs. 3 and 4, respectively. In Fig. 3, the ^{29}Si NMR spectra become complicated due to the overlapping of the peak maxima of mesoporous phases with the peak maxima of microporous phases. However, five different peaks centered at −99.4, −104.0, −110.7, −110.9

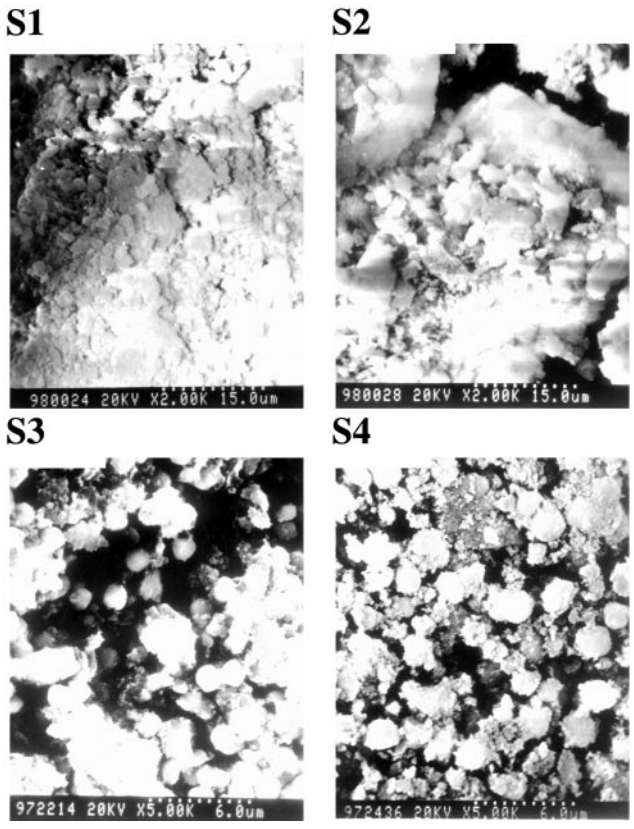

Fig. 2 Scanning electron micrographs of Beta/MCM-41 composites.

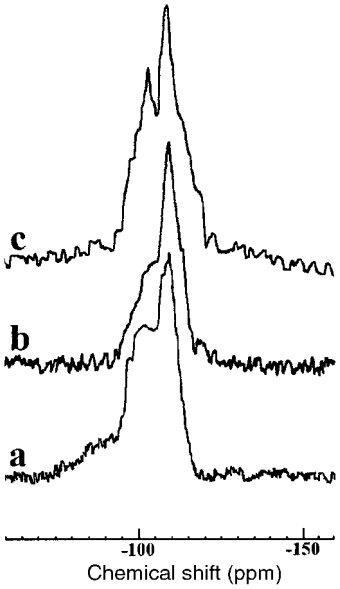

Fig. 3 ^{29}Si MAS NMR spectra of Beta/MCM-41 composites: (a) calcined S2; (b) calcined S4; (c) as-synthesized S4.

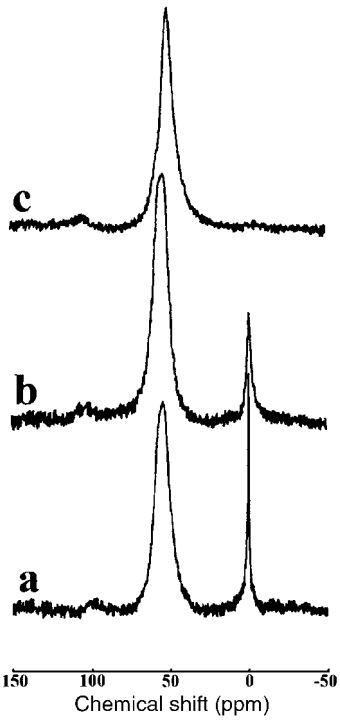

Fig. 4 ^{27}Al MAS NMR spectra of Beta/MCM-41 composites: (a) calcined S2; (b) calcined S4; (c) as-synthesized S4.

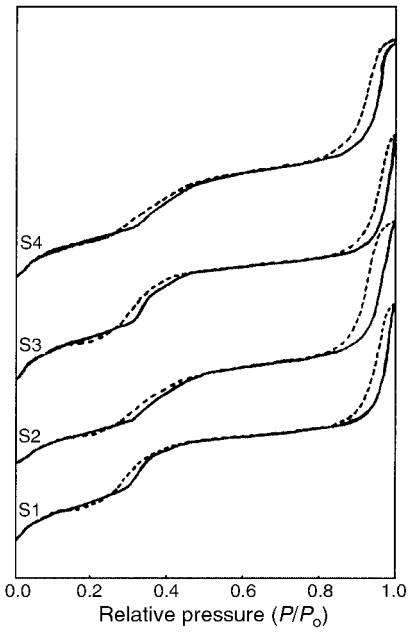

Fig. 5 Nitrogen adsorption (solid line) and desorption (dotted line) isotherms at 77 K on Beta/MCM-41 composites.

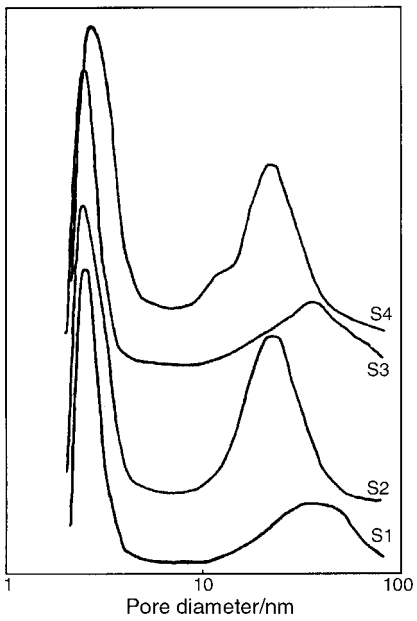

Fig. 6 BJH pore size distribution plots for Beta/MCM-41 composites.

and −115.1 ppm can be distinguished by Gaussian simulation. The peaks centered at −99.4 and −110.7 ppm correspond to Si atoms in Si (1Al) and Si (0Al) configurations in the mesoporous phases.[22,23] In the microporous phases, the peak maximum at −104.0 ppm can be assigned to the presence of Si atoms in Si (1Al) environments[24] and the other two peaks detected at −110.9 and −115.1 ppm are characteristic of non-equivalent silicon atoms in Si (0Al) environments.[25] In ^{27}Al MAS NMR spectra (Fig. 4), the peaks around 50 and 0 ppm are indicative of tetrahedrally coordinated aluminium in framework and octahedral non-framework aluminium, respectively. It is clear that the uncalcined composite, sample S4, exhibits only a peak at 55.0 ppm corresponding to tetrahedrally coordinated framework aluminium. After calcination at 823 K, it can be observed that the intensities of peaks of tetrahedrally coordinated aluminium decrease and the peaks corresponding to octahedral non-framework Al species appear for Beta/MCM-41 composites. Moreover, the degree of dealumination is reduced with increasing relative crystallinity of Beta in Beta/MCM-41 composites.

The N_2 adsorption–desorption isotherms and the BJH pore size distribution calculated from the analysis of the desorption branch of the isotherms for Beta/MCM-41 composites are presented in Figs. 5 and 6, respectively. It can be seen that all samples exhibit a typical irreversible type IV isotherm with two separate, well expressed H1 hysteresis loops, as defined by IUPAC,[26] at relative pressures P/P_0 of 0.20–0.45 and 0.8–1.0. Correspondingly, the pore size distribution reveals that there are two mesopore sizes in the composite, namely a bimodal distribution. The first condensation step on the isotherm at $P/P_0 = 0.20$–0.45 is characteristic of capillary condensation of framework-confined mesopores.[5,27] The second condensation step on the isotherm at $P/P_0 > 0.8$ indicates the presence of a significant amount of secondary mesopores contributed by the filling of interparticle spaces[28] and the particle sizes of the composites are quite uniform. Table 2 shows the textural properties of Beta/MCM-41 composites. It is obvious that there are similar BET surface areas and pore diameters for the mesoporous phases of the composites with various crystallinities of Beta. Nevertheless, the pore wall thickness in the mesoporous phases of the studied samples gradually increases from 1.91 nm to 2.24 nm as the a_0 parameter increases. Moreover, the surface areas contributed by Beta phases in the composites calculated with the *t*-plot and MP method increase with the increasing relative crystallinity of Beta. It is worth mentioning that the pore wall thickness in the mesoporous phases of the composites is in the range of 1.91–2.24 nm, which is unusually high compared with that of traditional mesoporous materials.[2,29] It can be suggested that the interaction between positively charged CTA^+ micelles and aluminosilicate anions is weakened by the large number of secondary building units, characteristic of zeolite Beta, in the mesopore wall, which brings about the increase in the pore wall thickness of the mesophase in Beta/MCM-41 composites.[18]

NH_3-TPD patterns of Beta/MCM-41 composites are shown in Fig. 7. The quantitative results of acidity are listed in Table 3. It can be seen that the composites with various crystallinities of Beta exhibit both the low-temperature peak at about 500 K for weak acid sites and the high-temperature broad peak at about 660 K for medium acid sites. The number of medium acid sites in the composites increases with the increasing relative crystallinity of Beta although the number of weak acid sites in the composites is almost identical under various crystallinities of Beta. Thus, the total number of acid

Table 2 Textural properties of Beta/MCM-41 composites

Sample	SiO_2/Al_2O_3	BET surface area/$m^2\ g^{-1}$	Micropore surface area/$m^2\ g^{-1}$	Mesoporous phase		
				Pore diameter *D*/nm	a_0[a]/nm	t[b]/nm
S1	25.8	522	90	2.61	4.52	1.91
S2	26.0	558	104	2.62	4.70	2.08
S3	25.5	503	115	2.64	4.88	2.24
S4	25.3	562	140	2.74	4.91	2.17

[a]Unit cell parameter calculated as $a_0 = 2d_{100}/\sqrt{3}$. [b]Pore wall thickness, $t = a_0 - D$.

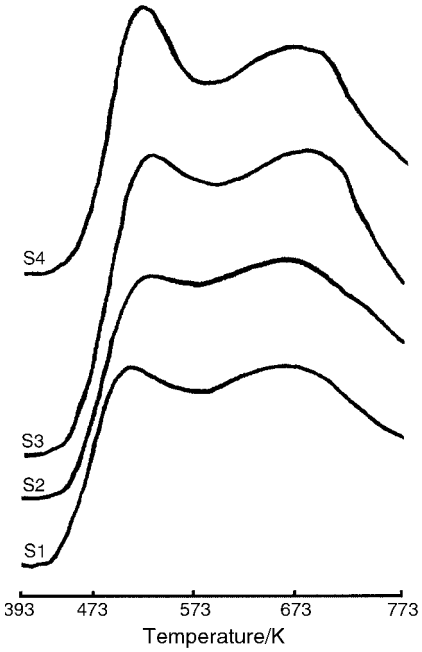

Fig. 7 NH_3-TPD patterns of Beta/MCM-41 composites.

sites on the composites increases with increasing relative crystallinity of Beta.

Table 3 shows the catalytic activities for n-heptane cracking at 673 K over different Beta/MCM-41 composites. The composite with the highest crystallinity of Beta (39%, sample S4) exhibits the highest catalytic activity; while the composite with only 16% crystallinity of Beta (sample S1) shows the lowest catalytic activity in spite of its comparable weak acidity. From Table 3, it can be seen that the higher the crystallinity of Beta in the sample, the higher catalytic activity the sample has. This observation means that the medium acid sites, rather than the weak ones, are the active sites for the reaction of n-heptane cracking. This result is in excellent agreement with the NH_3-TPD data.

It should be noted that the number and strength of the acid sites for the catalyst can be tailored by controlling the crystallinity of the catalyst to meet the acidity demands of different catalytic reactions. In addition, it is imperative to select a good probe molecule in making the best use of the two-fold pore systems and distinctive acid sites in Beta/MCM-41 composites. Detailed studies of potential applications for these composites are in progress.

4. Conclusions

A two-step crystallization approach involving combination of low crystallinity zeolite Beta gel with CTAB surfactant solution has been employed to synthesize a series of Beta/MCM-41 composites with relative crystallinities of Beta from 16 to 39%. The composites all possess bimodal mesopore systems and microporous structures of zeolite Beta. Interestingly, the pore wall thickness in the mesoporous phases of Beta/MCM-41 composites is in the range of 1.91–2.24 nm, which is unusually high compared with that of traditional mesoporous materials. With increasing crystallinity of Beta, the number of medium acid sites increases. Correspondingly, composites with higher Beta crystallinity exhibit higher catalytic activity for n-heptane cracking.

Table 3 Acidity of Beta/MCM-41 composites measured by NH_3-TPD and catalytic activity for n-heptane cracking at 673 K

	Peak temp./K		Acidity ($\times 10^{20}$ g^{-1})			
Sample	I	II	I	II	I+II	n-Heptane conversion[a] (%)
S1	498	654	0.77	1.07	1.84	51
S2	517	652	0.75	1.16	1.91	63
S3	519	676	0.81	1.27	2.08	75
S4	507	664	0.87	1.43	2.30	84

[a]The conversion of n-heptane during cracking over zeolite Beta under the same conditions is 95%.

Acknowledgements

We are grateful to the National Natural Science Foundation of China for financial support (Grant No. 29733070).

References

1 C. T. Kresge, M. E. Leonowicz, W. J. Roth, J. C. Vartuli and J. S. Beck, *Nature*, 1992, **359**, 710.
2 J. S. Beck, J. C. Vartuli, W. J. Roth, M. E. Leonowicz, C. T. Kresge, K. D. Schmitt, C. T.-W. Chu, D. H. Olson, E. W. Sheppard, S. B. McCullen, J. B. Higgins and J. L. Schlenker, *J. Am. Chem. Soc.*, 1992, **114**, 10834.
3 M. E. Davis, *Nature*, 1993, **364**, 391.
4 R. Mokaya, W. Jones, Z. Luan, M. D. Alba and J. Klinowski, *Catal. Lett.*, 1996, **37**, 113.
5 X. Chen, L. Huang, G. Ding and Q. Li, *Catal. Lett.*, 1997, **44**, 123.
6 X. Zhao, G. Q. Lu and G. J. Millar, *Ind. Eng. Chem. Res.*, 1996, **35**, 2075.
7 A. Corma, *Chem. Rev.*, 1997, **97**, 2373.
8 K. R. Kloetstra, H. W. Zandbergen, J. C. Jansen and H. van Bekkum, *Microporous Mater.*, 1996, **6**, 287.
9 K. R. Kloetstra, J. C. Jansen and H. van Bekkum, *Prepr. Am. Chem. Soc., Div. Pet. Chem.*, 1996, **41**, 412.
10 K. R. Kloetstra, H. van Bekkum and J. C. Jansen, *Chem. Commun.*, 1997, 2281.
11 A. Karlsson, M. Stöcker and R. Schmidt, *Microporous Mesoporous Mater.*, 1999, **27**, 181.
12 L. Huang, Ph.D. thesis, Fudan University, 1997.
13 L. Huang, W. Guo, P. Deng, Z. Xue and Q. Li, *J. Phys. Chem. B*, 2000, **104**, 2817.
14 J. Perez-Pariente, J. A. Martens and P. A. Jacobs, *Appl. Catal.*, 1987, **31**, 35.
15 M. A. Camblor, A. Mifsud and J. Perez-Pariente, *Zeolites*, 1991, **11**, 792.
16 M. A. Camblor and J. Perez-Pariente, *Zeolites*, 1991, **11**, 202.
17 W. Guo, L. Huang, H. Chen and Q. Li, *Chem. J. Chin. Univ.*, 1999, **20**, 356.
18 W. Guo, L. Huang, P. Deng, Z. Xue and Q. Li, *Microporous Mesoporous Mater.*, 2001, in press.
19 B. C. Lippens and J. H. De Boer, *J. Catal.*, 1965, **4**, 319.
20 R. Sh. Mikhail, S. Brunauer and E. E. Boder, *J. Colloid Interface Sci.*, 1968, **26**, 45.
21 J. B. Higgins, R. B. LaPierre, J. L. Schlenker, A. C. Rohrman, J. D. Wood, G. T. Kerr and W. J. Rohrbaugh, *Zeolites*, 1988, **8**, 446.
22 R. Ryoo and J. M. Kim, *J. Chem. Soc., Chem. Commun.*, 1995, 711.
23 A. Steel, S. W. Carr and M. W. Anderson, *Chem. Mater.*, 1995, **7**, 1829.
24 C. Jia, P. Massiani and D. Barthomeuf, *J. Chem. Soc., Faraday Trans.*, 1993, **89**, 3659.
25 J. Perez-Pariente, J. Sanz, V. Fornes and A. Corma, *J. Catal.*, 1990, **124**, 217.
26 K. S. W. Sing, D. H. Everett, R. A. W. Haul, L. Moscou, R. A. Pierotti, J. Rouquerol and T. Siemieniewska, *Pure Appl. Chem.*, 1985, **57**, 603.
27 X. Chen, L. Huang and Q. Li, *J. Phys. Chem. B*, 1997, **101**, 8460.
28 M. A. Camblor, A. Corma and S. Valencia, *Microporous Mesoporous Mater.*, 1998, **25**, 59.
29 A. Monnier, F. Schüth, Q. Huo, D. Kumar, D. Margolese, R. S. Maxwell, G. D. Stucky, M. Krishnamurty, P. Petroff, A. Firouzi, M. Janicke and B. F. Chmelka, *Science*, 1993, **261**, 1299.